Nihon Reoroji Gakkaishi Vol.50, No.1, 73~82
(Journal of the Society of Rheology, Japan)

DOI: 10.1678/rheology.50.73

Invited Review

Rheological Properties of Nanocellulose Dispersions in the Dilute Region: Current Understanding and Future Perspectives

Reina TANAKA†

Forestry and Forest Products Research Institute, Forest Research and Management Organization, 1 Matsunosato, Tsukuba, Ibaraki 305-8687, Japan
(Received : September 29, 2021)

The current knowledge and prospects for rheological properties of nanocellulose dispersions in a dilute region are presented. It is essential to clarify the rheological properties of dilute nanocellulose dispersions because they represent the properties of nanocellulose. This study highlights intrinsic viscosity and viscoelastic relaxation, which are indicators of average size, size distribution, and flexibility. While the intrinsic viscosity and viscoelastic relaxation of rod-shaped cellulose nanocrystals (CNCs) can be explained by existing theories of polymers, those of cellulose nanofibers (CNFs) are not fully understood because of their kinks and flexibility.
Key Words: Nanocellulose / Intrinsic viscosity / Viscoelasticity / Relaxation

1. INTRODUCTION

The formation of a sustainable society by using biological resources has become a necessity with the adoption of the Sustainable Development Goals at the UN Summit in 2015. Particularly, nanocellulose, a new nanomaterial derived from abundant forest resources, has excellent properties such as high crystal moduli[1-3], high strength[4], low thermal expansion[5], lightweight, and biological compatibility, and is expected to be implemented in society in various fields beyond the scope of conventional cellulose use.

Nanocellulose is classified into rod-shaped cellulose nanocrystals (CNCs) and cellulose nanofibers (CNFs). In the case of CNFs, various preparation methods are developed, and their compositions and structures are diversified accordingly[6]. Recently, the ISO/TC229 Nanotechnologies Technical Committee published international standards on preparation and quality evaluation methods for CNCs and individualized CNFs[7, 8]. Nanocellulose is commonly available as aqueous dispersions. However, the rheological properties of nanocellulose dispersions in the dilute region have not yet been fully clarified although they reflect characteristics of nanocellulose.

In the case of polymers, intrinsic viscosity is widely used as a basic parameter of molecular weight and flexibility in liquids. Therefore, intrinsic viscosities of nanocellulose dispersions can be used to evaluate the average size of nanocellulose. The average size and size distributions of nanocellulose are still commonly determined by microscopically evaluating a finite number of nanocellulose fibers, which is a time-consuming and highly specialized technique. In contrast, the intrinsic viscosity of nanocellulose dispersions can be easily evaluated at the industrial level using a simple viscometer. In the field of polymer science, the relaxation time, or the time to return from non-equilibrium to equilibrium through thermal motions, is widely studied. Relaxation times in the dilute region reflect polymer size distributions and flexibility, and they are useful for optimizing molding processes and material designs. However, because of the extremely low viscoelasticity of dilute nanocellulose dispersions, their relaxation behavior is little known. The relaxation behavior of nanocellulose should be clarified to promote its industrial use.

In this study, we focus on current understandings of the intrinsic viscosities and viscoelastic relaxation of nanocellulose, especially CNCs and individualized CNFs, in the dilute region. The relationship between average aspect ratios and intrinsic viscosities of nanocellulose is mainly discussed in Section 2. Recent progress on the viscoelastic relaxation of nanocellulose is outlined in Section 3. Finally, we discuss the current challenges and future perspectives in comprehensively understanding the rheological properties of nanocellulose

† Corresponding author.
E-mail : tanakar1101@ffpri.affrc.go.jp
Tel: + 81-29-829-8270

dispersions in the dilute region.

2. INTRINSIC VISCOSITY

2.1 Introduction

Viscosity η of polymer solutions is expressed as a function of the weight of a polymer in unit volume, c.

$$\eta = \eta_s\{1 + [\eta]c + k'([\eta]c)^2 + \cdots\} \quad (1)$$

where η_s is the solution viscosity. The c of the polymer is expressed as

$$c = \frac{M}{N_A}\nu \quad (2)$$

where M is the molar mass of the polymer, N_A is the Avogadro number, ν is the number density of the polymer.

$[\eta]$ and k' are termed as the intrinsic viscosity and the Huggins' coefficient, respectively. $[\eta]$ is a measure of the contribution of polymers to solution viscosity, which reflects molecular weights and flexibility of polymers. Eq. 1 is written as follows;

$$\frac{\eta-\eta_s}{\eta_s c} \equiv \frac{\eta_{sp}}{c} = [\eta]\{1 + k'[\eta]c + \cdots\} \quad (3)$$

where η_{sp} represent the specific viscosity. Ideally, $[\eta]$ should be evaluated in the dilute region where each polymer can rotate freely and interactions between rods are negligible. However, in the case of dilute nanocellulose/water dispersions, it is difficult to evaluate their viscosities because of their extremely low viscosities (~1 mPa s). The k' of rigid and semiflexible polymers has been reported less than 0.5[9, 10]. Thus, $\frac{\eta_{sp}}{c}$ in eq. 3 can be approximated as $[\eta]$ when $[\eta]c$ is sufficiently less than 1.

The overlap critical number density (ν^*) or the critical concentration (c^*), which are the boundaries between the dilute and semi-dilute regions, are used as a measure to determine the dilute region. In the case of rod-like polymers, ν^* is theoretically defined as follows using the rod length (L)[11].

$$\nu^* = L^{-3} \quad (4)$$

Then, c^* of rods is given by

$$c^* = \rho V_c L^{-3} \quad (5)$$

where V_c is the volume of the rods and ρ is the density of the rods. The c^* can be experimentally determined by plotting η_{sp} as a function of c; the slopes drastically increase above the c^*[12].

Viscosities of nanocellulose dispersions can demonstrate shear-thinning behavior even in the dilute regime because of their rod-like structure. Thus, they should be measured at shear rates ($\dot{\gamma}$) where Brownian motions of rods are dominant rather than shear forces. The appropriate ranges of $\dot{\gamma}$ can be estimated using rotational Pèclet number (Pe_{ort})[13].

$$Pe_{ort} = \frac{\dot{\gamma}}{D_{r,0}} \quad (6)$$

The rotational diffusion coefficient ($D_{r,0}$) of rod-like particles at infinite dilution is given by

$$D_{r,0} = \frac{3k_B T(\ln(L/d)-\beta)}{\pi\eta_s L^3} \quad (7)$$

where η_s is the dispersion medium viscosity, k_B is the Boltzmann constant, T is the temperature, L is the rod length, d is the rod width, and β is a constant of the hydrodynamic interaction which depends on the shape of particles[11]. When $Pe_{ort} << 1$, Brownian motions of rods exceed shear forces, and rods are randomly oriented. However, shear forces exceed Brownian motions at $Pe_{ort} >> 1$, and rods are aligned with the shear flow. When measuring viscosities with a capillary viscometer, an adequate capillary should be carefully chosen so that the designated shear rates in the capillary are lower than $D_{r,0}$ of samples[14]. Recently, several researchers have estimated $D_{r,0}$ using average dimensions determined by microscopy and confirmed that Pe_{ort} in capillaries were lower than 1[15, 16]. Ranges of shear rates at $Pe_{ort} << 1$ can be determined visually in the case of shear viscosity measurement because viscosities are measured in a wide range of shear rates[17, 18].

2.2 Intrinsic viscosity of nanocellulose dispersions

Several researchers have intensively studied the evaluation of aspect ratios (p) of nanocellulose, especially rod-shaped CNCs, using theoretical equations for $[\eta]$ of ellipsoids/cylinders (Table I). Marchessault *et al.* conducted the first investigation on an S-CNC (see Table A1) approximately fifty years ago[19]. Average length of the S-CNC was estimated using Simha's formula (eq. A3)[20], describing the relationship between p and $[\eta]$ of ellipsoids, which were also used in several literature (Table I)[16, 19, 21-26]. The average length was ~30 % longer than those determined by microscopy. This is probably because the S-CNC had surface charges whereas non-charged ellipsoids are assumed in this formula.

Table I Summary of previous studies on intrinsic viscosity of nanocellulose dispersions.

	Sample[a]	Aspect ratio, p	Apparatus	Electroviscous effect[b]	Eqs.[c] used for p calculation	Ref.
Marchessault *et al.* (1961)	S-CNC	25	Ubbelohde viscometer	–	A3	19
Araki *et al.* (1998)	S-CNC H-CNC	50 ± 20	Double-cylinder type viscometer	–	A3	21
Bercea and Navard (2000)	S-CNC	140	Ubbelohde viscometer & Rheometer	–	–	14
Boluk *et al.* (2011)	S-CNC	30	Ubbelohde viscometer	+	A3	22
González-Labrada and Gray (2012)	S-CNC	30	Rolling-ball viscometer	+	–	28
Iwamoto *et al.* (2014)	S-CNC H-CNF	47 ± 24 207 ± 81 310 ± 90	Rheometer	–	A3	23
Jowkarderis *et al.* (2014)	T-CNF	115 ± 40	Ubbelohde viscometer	+	A6	15
Lenfant *et al.* (2015)	C-CNC	20 ± 10	Cannon Ubbelohde viscometer	+	A3	16
Li *et al.* (2015)	S-CNC	38 ± 15 49 ± 17 55 ± 20	Rheometer	–	A3	24
Tanaka *et al.* (2015)	T-CNC T-CNF	23–77 103–376	Rheometer	–	–	17
Tanaka *et al.* (2017)	S-CNC	77–112	Rheometer	+	–	18
Wu *et al.* (2017)	S-CNC	22 ± 5 22 ± 4	Ubbelohde viscometer	+	A5	29
Beuguel *et al.* (2018)	S-CNC	12.5	Rheometer	+	A3	25
Wu *et al.* (2019)	S-CNC	14 ± 3 32 ± 9	Ubbelohde viscometer	+	A5	30
Yamagata *et al.* (2020)	T-CNF	77 & 243	Rheometer	–	A3	26

[a] The details are shown in Table A1. [b] The symbols, + and –, represent the presence or absence of discussion on the primary electroviscous effect in the literature, respectively. [c] The details are shown in Table A2.

When shear forces are applied to surface-charged particles, the electric double layers surrounding the particles are deformed, which increases η and $[\eta]$ of the particle dispersions[27]. This is termed as a primary electroviscous effect. In the 2010s, the primary electroviscous effect of surface-charged nanocellulose was comprehensively investigated[15, 16, 22, 28-30]. When salts are added to surface-charged nanocellulose dispersions to the extent that the nanocellulose fibers do not aggregate, the electric double layers compress, reducing the primary electroviscous effect. Therefore, η and

$[\eta]$ of the particle dispersions decrease. The influences of the primary electroviscous effect on experimental $[\eta]$ of nanocellulose dispersions with $p < \sim 100$ determined by electron microscopy are summarized in Fig. 1. The $[\eta]$ in the absence of the primary electroviscous effect, which was measured using nanocellulose dispersions with salts, are well described by Simha's formula assuming non-charged particles[15, 16, 22, 29, 30]. It was found that the $[\eta]$ measured in the presence of the primary electroviscous effect were significantly higher than those without the effect. Therefore, when evaluating p of surface-charged nanocelluloses from $[\eta]$ using Simha's formula, it is necessary to measure $[\eta]$ with the primary electroviscous effect excluded. It is considered that the same holds for the other equations for the intrinsic viscosity of rod-like particles (Table A2)[13, 31-36].

When $[\eta]$ are evaluated from η measured using a rheometer, it is difficult to accurately measure η at $Pe_{ort} << 1$ in the dilute region because of their low viscosity. For the case of high-aspect-ratio CNFs, this problem is more critical than for CNCs, because the c^* of CNFs is lower. Several researchers have found that high-viscous dispersion media such as 50 % glycerol/water solution and 20 % polyethylene glycol (PEG)/water solution are effective at solving this problem[18, 25]. These organic solvents aqueous solutions also contributed to a decrease in the primary electroviscous effect. Beuguel *et al.* reported that $[\eta]$ of an S-CNC in 20 % PEG solution was lower than that in pure water (Fig. 1)[25]. Tanaka *et al.* reported that η of S-CNCs measured in 50 % glycerol solution with 10 mM NaCl almost overlapped with those measured without salts[18]. Although it must be studied, once suitable dispersants are found, the evaluation of $[\eta]$ of nanocellulose using a rheometer will become easier.

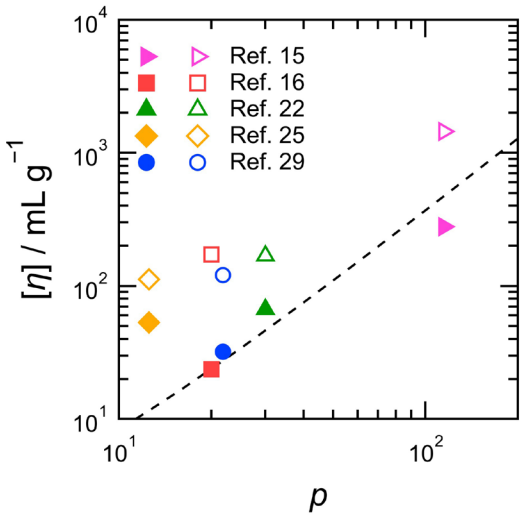

Fig. 1 The influences of the primary electroviscous effect on experimental intrinsic viscosities $[\eta]$ of nanocellulose samples with $p < \sim 100$. The dotted line represents Simha's formula (eq. A3). The open and filled symbols show $[\eta]$ measured with and without the primary electroviscous effect, respectively.

Yoshizaki and Yamakawa proposed an equation for $[\eta]$ of straight cylindrical polymers with hemispheroid caps at the ends in the dilute region[34].

$$[\eta] = (2\pi N_A d^3/45M)p^3 F_\eta(p,\varepsilon) \tag{8}$$

where $F_\eta(p, \varepsilon)$ is a parameter depending on the shape and size of cylinders. This equation is valid for spheroid cylindrical polymers of arbitrary size. In the case of rods, whose v is expressed as $\frac{c}{\rho V_c}$ based on eq. 2, eq. 8 is modified as follows;

$$[\eta] = (2\pi d^3/45\rho V_C)p^3 F_\eta(p,\varepsilon) \tag{9}$$

It was verified that whether the $[\eta]$ values of various CNCs and CNFs can be expressed by the classical theoretical equation, eq. 9. For simplicity, the theoretical calculations were made assuming that the hemispheroids at the ends were spherical ($\varepsilon = 1$). Eq. 9 was rewritten as follows to discuss $[\eta]$ solely as a function of p.

$$[\eta]\rho V_c d^{-3} = \frac{2\pi}{45} p^3 F_\eta(p,1) \tag{10}$$

Figure 2a shows $[\eta]\rho V_c d^{-3}$ values measured without the primary electroviscous effect. The theoretical $[\eta]\rho V_c d^{-3}$ values calculated using Simha's formula were also plotted in Fig. 2a for comparison of the formula with eq. 10. The $[\eta]\rho V_c d^{-3}$ values of low-aspect-ratio nanocellulose samples ($p < \sim 100$) measured without the primary electroviscous effect were slightly better described by eq. 10 than Simha's formula. The data for tunicate S-CNCs dispersed in 50 % glycerol solution confirmed that the primary electroviscous effect was sufficiently reduced by 50 % glycerol solution. These results show that $[\eta]\rho V_c d^{-3}$ of low-aspect-ratio nanocellulose samples ($p < \sim 100$) measured without the primary electroviscous effect can be expressed by the classical theory of $[\eta]$ for straight cylinders in the dilute region. One of the tunicate S-CNCs showed a different trend in the experimental $[\eta]\rho V_c d^{-3}$, which was probably due to kinks[18]. For nanocellulose samples measured with the primary electroviscous effect, the experimental $[\eta]\rho V_c d^{-3}$ values tended to be larger than their theoretical values regardless of p (Fig. 2b). The reason of this discrepancy for nanocellulose samples with $p < \sim 100$ can be explained by the primary electroviscous effect based on Fig. 1. However, the influences of the primary electroviscous effect on experimental $[\eta]\rho V_c d^{-3}$ values for high-aspect-ratio CNFs ($p > \sim 100$) have not yet been studied

much, and should be investigated. In the case of high-aspect-ratio CNFs, kinks and flexibility would also contribute to the larger estimation of their experimental $[\eta]\rho V_c d^{-3}$ values[37].

Existing theoretical equations for $[\eta]$ of rod-like particles do not take into account their flexibility and kinks (Table A2). Therefore, new equations to describe the relation between p and $[\eta]$ of not only CNCs but also CNFs are required from an industrial viewpoint. Tanaka *et al.* proposed an empirical equation to express $[\eta]$ for CNCs and CNFs (p = 20–380) as a function of p determined by microscopy, regardless of dimensions and flexibility[17]. The $[\eta]$ values of CNCs and CNFs in this study were evaluated in the presence of the primary electroviscous effect.

$$\rho[\eta] = 0.15p^{1.9} \tag{11}$$

Eq. 11 was modified as follows using dimensions of the CNCs and CNFs reported in this study for easier comparison with eq. 10.

$$[\eta]\rho V_c d^{-3} = 0.13p^{2.9} \tag{12}$$

Yamagata *et al.* investigated the reproductively of eq. 11 using surface-charged T-CNFs with p of 77 and 243[26]. The T-CNFs roughly obeyed the relation of eq. 11 (Fig. 3). However, the $[\eta]$ value of longer T-CNF (p = 243) may be underestimated because they evaluated $[\eta]$ from η at high shear rates (100 s^{-1}). According to dimensions reported in this study, the Pe_{ort} at 100 s^{-1} would be ~2.8. The plots for other samples (T-CNF, S-CNC, and H-CNF) reported in the literature are also shown in Fig. 3[23]. The experimental $[\eta]\rho V_c d^{-3}$ values of H-CNFs reported by Iwamoto *et al.* showed variations from eq. 12. According to the dimensions reported in this study, the $[\eta]$ value of longer H-CNF (p = ~310) would be calculated from η at $Pe_{ort} > 1$, which can result in a large discrepancy from eq. 12. The experimental $[\eta]\rho V_c d^{-3}$ value of a T-CNF measured by Jowkaderis *et al.* was in good agreement with the theoretical value calculated by eq. 12. Because the $[\eta]$ values of CNFs have not been studied as extensively as those of CNCs (Table I), more studies must construct a more universal equation.

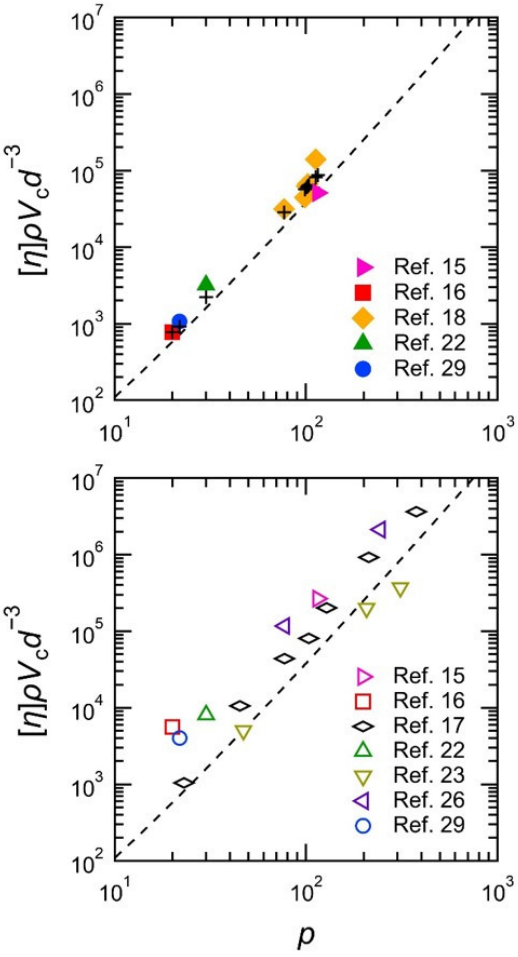

Fig. 2 Comparison of $[\eta]\rho V_c d^{-3}$ for various nanocellulose samples (p = 20–380) with eq. 10. The V_c and d values were calculated using dimensions reported in the literature. The ρ value is the density of cellulose (1.6 g mL^{-1}).The dashed line represents eq. 10. The filled and open symbols show $[\eta]\rho V_c d^{-3}$ values measured without and with the primary electroviscous effect, respectively. The cross points show theoretical $[\eta]\rho V_c d^{-3}$ values calculated using Simha's formula.

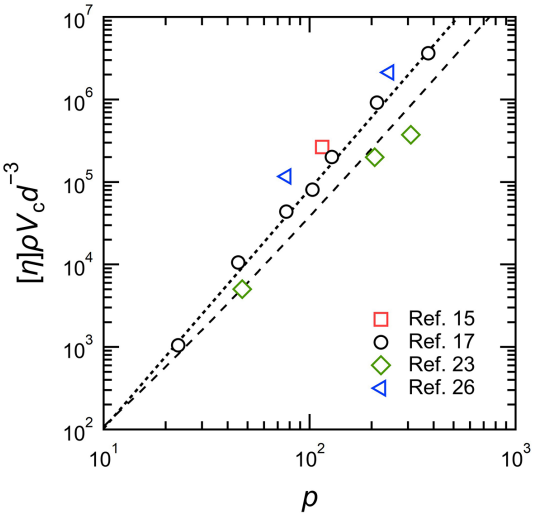

Fig. 3 Experimental $[\eta]\rho V_c d^{-3}$ vs. microscopy-determined aspect ratios p of nanocellulose reported in the literature. The V_c and d values were calculated using dimensions reported in the literature. The ρ value is the density of cellulose (1.6 g mL^{-1}). The dashed and dotted lines represent eq. 10 and 12, respectively. The $[\eta]$ values were measured in the presence of the primary electroviscous effect.

3. VISCOELASTIC RELAXATION

3.1 Introduction

In the field of polymer sciences, the dynamic viscoelasticity of rod-like polymers in the dilute region has been

extensively studied from experimental and theoretical aspects for approximately fifty years. The frequency dependence of reduced intrinsic storage and loss moduli at infinite dilution is given by

$$[G']_{\mathrm{R}} = (M/RT)\lim_{c\to 0} G'/c = m_1\omega^2{\tau_{\mathrm{rod},0}}^2\left(1+\omega^2{\tau_{\mathrm{rod},0}}^2\right)^{-1} \quad (13)$$

$$[G'']_{\mathrm{R}} = (M/RT)\lim_{c\to 0} (G''-\omega\eta_{\mathrm{s}})/c = \omega\tau_{\mathrm{rod},0}\left[m_1\left(1+\omega^2{\tau_{\mathrm{rod},0}}^2\right)^{-1}+m_2\right] \quad (14)$$

where M is the molecular weight, R is the gas constant. The numerical coefficients m_1 and m_2 depend on the shape of polymers. The details are described elsewhere[38]. Yamakawa proposed $m_1 = 3/5$ and $m_2 = \frac{4}{5\gamma} - \frac{3}{5}$ for the case of straight cylinders[33]. Yoshizaki and Yamakawa proposed $m_1 = 3\chi^2/5$ and $m_2 = \frac{4}{5\gamma}\left(1-\frac{3}{4}\chi^2\gamma\right)$ for the case of spheroid cylinders with hemispheroid caps at the ends[34]. The parameters γ and χ depend on the shape and aspect ratio of cylinders[33, 34]. The rotational relaxation time of rigid rods at infinite dilution ($\tau_{\mathrm{rod},0}$) is calculated from $D_{\mathrm{r},0}$.

$$\tau_{\mathrm{rod},0} = \frac{1}{6D_{\mathrm{r},0}} = \pi\eta_{\mathrm{s}}L^3/\{18k_{\mathrm{B}}T[\ln(L/d)-\beta]\} \quad (15)$$

The viscoelastic relaxation of CNCs and CNFs can be explained on the basis of eq. 13–15.

3.2 Viscoelastic relaxation of nanocellulose

Dynamic viscoelasticity of nanocellulose in the dilute region has barely been investigated compared with their intrinsic viscosities. This is because dilute nanocellulose/water dispersions have extremely low G' compared to G'', which makes it difficult to evaluate their viscoelasticity accurately. However, to promote the use of nanocellulose at the industrial level, it is necessary to evaluate relaxation behavior.

Only decades ago, Ishii *et al.* first reported frequency dependence of G' and G'' of surface-charged T-CNF/water dispersions[39, 40]. They used a T-CNF with a uniform width (~3 nm) and length distributions. They evaluated a longest relaxation time of the T-CNF as the inverse of a maximum frequency in the terminal relaxation region where $G' \sim \omega^2$ and $G'' \sim \omega$, using data of 0.02 % w/v T-CNF/water dispersion. They calculated the average length of the T-CNF from the longest relaxation time using eq. 15. However, the calculated length was one order of magnitude greater than the actual length determined by microscopy. There were several problems with the method used in this study to evaluate the average length from viscoelasticity. First, it was unclear whether the longest relaxation time corresponded to $\tau_{\mathrm{rod},0}$. To confirm this, it is desirable to measure the changes in τ_{rod} around c^*, which was conducted in recent studies[41, 42]. Second, longer fibers in the length distribution may influence the longest relaxation time. Third, the longest relaxation time determined at 0.02 % w/v may not be accurately measured because of their low viscoelasticities; the raw viscoelastic data of the T-CNF/water dispersions were scattered at c lower than 0.04 % w/v. Thus, it is necessary to use high viscosity dispersion media in order to accurately measure the viscoelasticity of nanocellulose in the dilute region.

Tanaka *et al.* measured viscoelasticity of CNCs (T-CNC and S-CNC) dispersed in high-viscous glycerol[43]. CNCs, which are conventionally considered rigid rods, were used as samples for easier investigations. According to small-angle light scattering (SAXS) measurements, CNCs were individually dispersed in glycerol as in water. The viscoelasticity of CNCs in the dilute region can be measured from –15 ºC to 25 ºC using glycerol as a dispersant, and the time–temperature superposition principle was applicable to the CNC/glycerol system. The G' and G'' values of CNCs at –15 ºC and 5 ºC overlapped those at 25 ºC by shifting them on the horizontal axis using shifting factors (a_{T}). The plots of a_{T} values against the inverse of temperature for the CNC/glycerol dispersions showed the same trends as glycerol (Fig. A1). The temperature dependences of a_{T} values for glycerol and CNC/glycerol dispersions were represented by the Arrhenius-type relationship.

$$\log a_{\mathrm{T}} = -\mathrm{A}\left(\frac{1}{T}-\frac{1}{T_{\mathrm{ref}}}\right) \quad (16)$$

where A is a material-specific constant, T_{ref} is the reference temperature. These results showed that the temperature dependence of the dispersion medium viscosity governed the viscoelasticity of the CNCs. Notably, CNCs showed relaxation behavior similar to semiflexible polymers; viscoelastic relaxation of the CNCs was well fitted by a theory for viscoelasticity of semiflexible polymers at infinite dilution by assuming the persistence length (L_{p}) as ~58 and ~2 μm for tunicate and softwood CNCs, respectively. The CNCs had viscoelastic relaxations derived from internal motions at high frequencies in addition to those derived from rigid rods' rotational motions at low frequencies (Fig. 4). Note that the theoretical fitting to the viscoelastic data was conducted by considering the length distributions of the CNCs determined by microscopy. The contributions of rotational (orientational)

motions of rigid rods to complex shear moduli (G_{ort}^{*}) reflected length distributions of the CNCs; that is, length distributions of the CNCs can be evaluated from the relaxation of rotational motions of rigid rods. The details of the theory are described elsewhere[44]. Although CNCs are substantially rigid, internal motions such as tension and curvature have been ovserved. However, the apparent Young's moduli (E = 0.4 GPa) of the tunicate and softwood CNCs estimated from L_p values were several orders of magnitude lower than previously-reported E values. This is probably because the apparent E was calculated by assuming CNCs had a homogeneous rectangular-prismatic structure, whereas actual CNCs have right-handled twists[37, 45–48]. This point is still unresolved.

Hasegawa *et al.* investigated the dynamic viscoelasticity of an S-CNC with a significant narrow length distribution[41]. An aqueous sucrose solution at 60 wt%, whose viscosity is approximately 50 times higher than pure water at 25 °C, was used as a dispersion medium. The viscoelastic measurements were conducted in an isotropic liquid state in the semi-dilute region. They determined several fundamental viscoelastic parameters from the viscoelastic data: the zero-shear viscosity ($\eta_0 = \lim_{\omega\to 0}\frac{G''}{\omega}$), the high frequency limiting viscosity ($\eta_\infty = \lim_{\omega\to\infty}\frac{G''}{\omega}$), an elastic coefficient ($A_G = \lim_{\omega\to 0}\frac{G'}{\omega^2}$), the rotational relaxation time of rigid rods [$\tau_{rod} = 5(\eta_0 - \eta_\infty)/3\nu k_B T$], the inverse of the steady-state compliance [$J_e^{-1} = (\eta_0 - \eta_\infty)^2/A_G$], and the average relaxation time [$\tau_w = (\eta_0 - \eta_\infty)J_e$]. The τ_w was determined from an intersecting point between $A_G(a_T\omega)^2$ and $(\eta_0 - \eta_\infty)a_T\omega$. With decreasing concentration, the τ_w values were empirically consistent with the τ_{rod} values and approached the $\tau_{rod,0}$ determined by dynamic light scattering (DLS) measurement. The experimental G' and G'' values at low concentrations near c^* approximately fitted by their theoretical values calculated from the obtained τ_w and J_e^{-1} values based on eq. 13–15. The terminal relaxation of the relatively dilute S-CNC dispersions near c^* can be explained by the theory for viscoelasticity of rod-like polymers with a single relaxation mode[49]. They also indicated the existence of fast relaxation modes at high frequencies derived from internal motions, which was consistent with the results of Tanaka et al[43].

Matsuo *et al.* investigated the dynamic viscoelasticity of a T-CNF with a wide length distribution in the semi-dilute region using Hasegawa *et al.* method[42]. They extended theoretical equations of τ_{rod} for monodisperse rigid rods to those for polydisperse rigid rods as follows, and demonstrated that these equations can be applied to the polydisperse T-CNF.

$$G' = \frac{3}{5}k_B T\omega^2 \sum_{i=1}^{n}\frac{\nu_i {\tau_{rod,i}}^2}{1+\omega^2{\tau_{rod,i}}^2} \tag{17}$$

$$G'' = \frac{3}{5}k_B T\omega \sum_{i=1}^{n}\frac{\nu_i \tau_{rod,i}}{1+\omega^2{\tau_{rod,i}}^2} + \eta_\infty\omega \tag{18}$$

They also defined the average rotational relaxation time of rigid rods $\langle\tau_{rod}\rangle$.

$$\langle\tau_{rod}\rangle = \frac{\sum_{i=1}^{n}\nu_i\tau_{rod,i}}{\nu} = \frac{5(\eta_0-\eta_\infty)}{3\nu k_B T} = \frac{5(\eta_\infty-\eta_S)}{3\nu k_B T} \tag{19}$$

where ν is the total number density of the T-CNF. They found that as solid concentrations decreased, $\langle\tau_{rod}\rangle$ approached the $\tau_{rod,0}$ determined by DLS measurement. However, the τ_w values were several times longer than the $\langle\tau_{rod}\rangle$ values, unlike in the case of the S-CNC, which had a significant narrow length distribution. The relaxation derived from the internal motions of CNFs has not yet been unrevealed. CNFs have defects

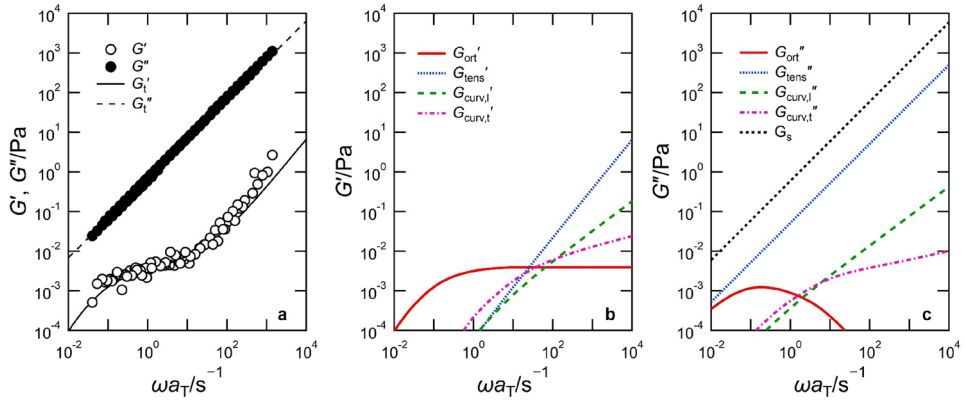

Fig. 4 (a) Comparison of experimental G^* for a tunicate S-CNC/glycerol dispersion with the theory for semiflexible polymers at infinite dilution. The orientation of rods (*ort*), tension (*tens*), and curvature (*curv, l* and *curv, t*) contributions to storage moduli (G_t') and loss moduli (G_t'') are shown in panels b and c, respectively. The viscoelastic data are presented in a composite curve form, which is produced by the time–temperature superposition principle. The reference temperature is 25 °C. Reprinted with permission from Tanaka R., Kashiwagi Y., Okada Y., and Inoue, T., Viscoelastic Relaxation of Cellulose Nanocrystals in Fluids: Contributions of Microscopic Internal Motions to Flexibility. *Biomacromolecules* **2020**. Copyright 2021 American Chemical Society.

such as kinks, which may be introduced during preparation[37, 50]. This makes it more complicated to investigate the internal motions of CNFs. Recently, properties of single cellulose nanofibrils, such as structures of twisted and kinked regions, as well as elastic responses, have been extensively studied using microscopy and simulations[37, 45, 48, 51-53]. These findings on single cellulose nanofibrils will aid in clarifying the overall viscoelastic relaxation of CNFs.

4. CONCLUSIONS AND PERSPECTIVES

This study focused on the intrinsic viscosities and viscoelastic relaxation of nanocellulose dispersions in the dilute region. The intrinsic viscosities of nanocelluloses, particularly for CNCs, have been extensively investigated. The aspect ratios of nanocelluloses with $p < \sim 100$ can be calculated from their intrinsic viscosities without the primary electroviscous effect, using classical equations for non-charged rod-like particles such as Simha's formula. However, it was difficult to evaluate aspect ratios of high-aspect-ratio CNFs ($p > \sim 100$) using the classical equations because of their flexibility and kinks. An empirical equation was proposed to express the relation between aspect ratios and intrinsic viscosities for nanocelluloses with $p < \sim 380$. However, there are only a limited number of CNF examples. Further studies on intrinsic viscosities of CNFs must construct a universal equation to describe intrinsic viscosities of nanocellulose regardless of dimensions and flexibility. If we can develop such a universal equation, intrinsic viscosities will be a strong tool to characterize nanocellulose quickly at the industrial level.

The viscoelastic relaxation of nanocellulose has received less attention than intrinsic viscosity because of the extremely low viscoelasticity of dilute nanocellulose/water dispersions. Instead of pure water, high-viscous dispersion media such as glycerol and 60 % sucrose solution are required. It was found that the theory for the viscoelasticity of semiflexible polymers at infinite dilution can describe the viscoelastic relaxation of CNCs. The relaxation modes derived from internal motions such as tension and curvature was firstly demonstrated by dynamic viscoelastic measurement, which were not found in intrinsic viscosities. However, the viscoelastic relaxation of CNFs, especially internal motions, is still under investigation. This is because CNFs have flexibility and kinks. The recent knowledge on the structures and mechanical properties of single cellulose nanofibrils would contribute to the understanding of the overall relaxation of CNFs.

5. APPENDIX

Table A1 The abbreviated terms of nanocellulose samples and their preparation conditions.

Abbreviations	Preparation conditions
S-CNC	sulfuric acid hydrolysis
H-CNC	hydrochloric acid hydrolysis
T-CNC	2,2,6,6-tetramethylpiperidine-1-oxyl (TEMPO)-oxidation & hydrochloric acid hydrolysis
C-CNC	Two-step oxidation
H-CNF	Fibrillation using a high pressure homogenizer
T-CNF	TEMPO-oxidation

Table A2 Theoretical equations for intrinsic viscosities of rod-like particles reported in the literature.

		Equations	Conditions	Ref.
A1	Onsager (1932)	$[\eta] = \frac{4}{15}\frac{p^2}{\ln p}$	prolate spheroids ($p >> 1$, $Pe_{ort} << 1$)	31
A2	Kuhn and Kuhn (1945)	$[\eta] = \frac{p^2}{5}\left(\frac{1}{3(\ln 2p - 1.5)} + \frac{1}{\ln 2p - 0.5}\right) + 1.6$	prolate spheroids ($p > 15$, $Pe_{ort} << 1$)	32
A3	Simha (1940)	$[\eta] = \frac{p^2}{5}\left(\frac{1}{3(\ln 2p - 1.5)} + \frac{1}{\ln 2p - 0.5}\right) + \frac{14}{15}$	ellipsoids ($p >> 1$)	20
A4	Yamakawa (1974)	$[\eta] = \frac{2\pi L^3}{45\,(\ln(p) - \beta)}\frac{1}{\rho V_C}$	straight cylinders ($L \to \infty$)	33
		$[\eta] = \frac{2\pi L^3}{45}\frac{1}{\rho V_C}\varepsilon f(\varepsilon)$		
A5	Parra-Vasquez *et al.* (2007)	$\varepsilon = 1/\ln 2p$	cylinders	35
		$f(\varepsilon) = \frac{1 + 0.64\varepsilon}{1 - 1.5\varepsilon} + 1.659\varepsilon^2$		
A6	Mansfield *et al.* (2008)	$[\eta] = \frac{8}{45}\frac{p^2}{\ln p}$	cylinders ($p \to \infty$)	36

*β: the hydrodynamic interaction V_c: the volume of a particle

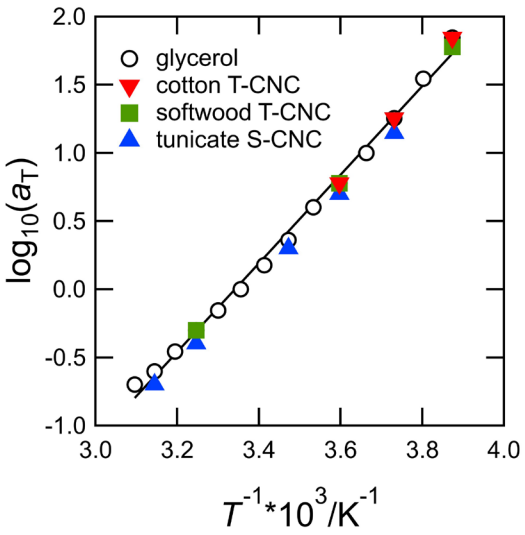

Fig. A1 The shifting factors (a_T) vs. the inverse of temperature for glycerol and CNC/glycerol dispersions. The reference temperature is 25 °C. The line shows the fitting result of the Arrhenius-type relationship to the data of glycerol. Adapted with permission from Tanaka R., Kashiwagi Y., Okada Y., and Inoue, T., Viscoelastic Relaxation of Cellulose Nanocrystals in Fluids: Contributions of Microscopic Internal Motions to Flexibility. *Biomacromolecules* **2020**. Copyright 2021 American Chemical Society.

ACKNOWLEDGEMENTS

The author acknowledges financial support from JSPS KAKENHI Grant Number JP20K15348. Dr. Yousuke Goi in DKS Co. Ltd., Dr. Kazuho Daicho in Graduate School of Agricultural and Life Sciences, The University of Tokyo, and Dr. Kazuma Miyagi in Forestry and Forest Products Research Institute are acknowledged for helpful discussions and valuable advice of this review.

REFERENCES

1) Sakurada I, Nukushina Y, Ito T, *J Polym Sci*, **57**, 651 (1962).
2) Šturcová A, Davies G R, Eichhorn S J, *Biomacromolecules*, **6**, 1055 (2005).
3) Wohlert J, Bergenstråhle-Wohlert M, Berglund L A, *Cellulose*, **19**, 1821 (2012).
4) Saito T, Kuramae R, Wohlert J, Berglund L A, Isogai A, *Biomacromolecules*, **14**, 248 (2013).
5) Hori R, Wada M, *Cellulose*, **12**, 479 (2005).

6) Lavoine N, Desloges I, Dufresne A, Bras J, *Carbohydr Polym*, **90**, 735 (2012).
7) ISO, ISO/TS 21346:2021 Nanotechnologies–Characterization of individualized cellulose nanofibril samples (2021).
8) ISO, ISO/TR 19716:2016 Nanotechnologies–Characterization of cellulose nanocrystals (2016).
9) Kasabo F, Kanematsu T, Nakagawa T, Sato T, Teramoto A, *Macromolecules*, **33**, 2748 (2000).
10) Itou T, Chikiri H, Teramoto A, Aharoni SM, *Polym J*, **20**, 143 (1988).
11) Doi M, Edwards SF, *"The theory of polymer dynamics"*, (1986), Oxford University Press New York.
12) Tanaka R, Saito T, Ishii D, Isogai A, *Cellulose*, **21**, 1581 (2014).
13) Wierenga AM, Philipse AP, *Colloids Surf, A*, **137**, 355 (1998).
14) Bercea M, Navard P, *Macromolecules*, **33**, 6011 (2000).
15) Jowkarderis L, van de Ven TG, *Cellulose*, **21**, 2511 (2014).
16) Lenfant G, Heuzey M, van de Ven T, Carreau P, *Cellulose*, **22**, 1109 (2015).
17) Tanaka R, Saito T, Hondo H, Isogai A, *Biomacromolecules*, **16**, 2127 (2015).
18) Tanaka R, Kuribayashi T, Ogawa Y, Saito T, Isogai A, Nishiyama Y, *Cellulose*, **24**, 3231 (2017).
19) Marchessault R, Morehead F, Koch MJ, *J Colloid Sci*, **16**, 327 (1961).
20) Simha R, *J Phys Chem*, **44**, 25 (1940).
21) Araki J, Wada M, Kuga S and Okano T, *Colloids Surf, A*, **142**, 75 (1998).
22) Boluk Y, Lahiji R, Zhao L, McDermott MT, *Colloids Surf, A*, **377**, 297 (2011).
23) Iwamoto S, Lee S-H, Endo T, *Polym J*, **46**, 73 (2014).
24) Li M, Wu Q, Song K, Lee S, Qing Y, Wu Y, *ACS Sustainable Chem Eng*, **3**, 821 (2015).
25) Beuguel Q, Tavares JR, Carreau PJ, Heuzey M-C, *J Rheol*, **62**, 607 (2018).
26) Yamagata Y, Suga K, Nakano Y, Takasaki Y, Miyamoto K, *Nihon Reoroji Gakkaishi (J Soc Rheol Jpn)*, **48**, 207 (2020).
27) Adachi Y, Kawashima YT, Ghazali MEB, *KONA*, **37**, 145 (2020).
28) González-Labrada E, Gray DG, *Cellulose*, **19**, 1557 (2012).
29) Wu Q, Li X, Fu S, Li Q, Wang S, *Cellulose*, **24**, 3255 (2017).
30) Wu Q, Li X, Li Q, Wang S, Luo Y, *Polymers*, **11**, 781 (2019).
31) Onsager L, *Phys Rev*, **40**, 1028 (1932).
32) Kuhn W, Kuhn H, *Helv Chim Acta*, **28**, 97 (1945).
33) Yamakawa H, *Macromolecules*, **8**, 339 (1975).
34) Yoshizaki T, Yamakawa H, *J Chem Phys*, **72**, 57 (1980).
35) Parra-Vasquez ANG, Stepanek I, Davis VA, Moore VC, Haroz EH, Shaver J, Hauge RH, Smalley RE, Pasquali M, *Macromolecules*, **40**, 4043 (2007).
36) Mansfield ML, Douglas JF, *Macromolecules*, **41**, 5422 (2008).
37) Usov I, Nyström G, Adamcik J, Handschin S, Schütz C, Fall A, Bergström L, Mezzenga R, *Nat Commun*, **6**, 7564 (2015).
38) Ferry JD, *"Viscoelastic properties of polymers."*, 3rd ed, (1980), John Wiley & Sons: New York.
39) Ishii D, Saito T, Isogai A, *Biomacromolecules*, **12**, 548 (2011).
40) Ishii D, Saito T, Isogai A, *Biomacromolecules*, **13**, 1706 (2012).
41) Hasegawa H, Horikawa Y, Shikata T, *Macromolecules*, **53**, 2677 (2020).
42) Matsuo F, Horikawa Y, Shikata T, *Nihon Reoroji Gakkaishi (J Soc Rheol Jpn)*, **49**, 179 (2021).
43) Tanaka R, Kashiwagi Y, Okada Y, Inoue T, *Biomacromolecules*, **21**, 408 (2020).
44) Shankar V, Pasquali M, Morse DC, *J Rheol*, **46**, 1111 (2002).
45) Ogawa Y, *Nanoscale*, **11**, 21767 (2019).
46) Paavilainen S, Róg T, Vattulainen I, *J Phys Chem B*, **115**, 3747 (2011).
47) Orts W, Godbout L, Marchessault R, Revol J-F, *Macromolecules*, **31**, 5717 (1998).
48) Willhammar T, Daicho K, Johnstone DN, Kobayashi K, Liu Y, Midgley PA, Bergström L, Saito T, *ACS nano*, **15**, 2730 (2021).
49) Doi M, Edwards S, *J Chem Soc, Faraday Trans 2*, **74**, 560 (1978).
50) Nyström G, Arcari M, Adamcik J, Usov I, Mezzenga R, *ACS nano*, **12**, 5141 (2018).
51) Uetani K, Uto T, Suzuki N, *Sci Rep*, **11**, 790 (2021).
52) Chen P, Ogawa Y, Nishiyama Y, Ismail AE, Mazeau K, *Phys Chem Chem Phys*, **18**, 19880 (2016).
53) Arcari M, Zuccarella E, Axelrod R, Adamcik J, Sánchez-Ferrer A, Mezzenga R, Nyström G, *Biomacromolecules*, **20**, 1288 (2019).